

# Renormalization of dispersion in electron-doped bilayer cuprate superconductors

Shuning Tan<sup>1\*</sup>, Yiqun Liu<sup>2</sup>, Yingping Mou<sup>3</sup>, Huaiming Guo<sup>4</sup>, and Shiping Feng<sup>5†</sup>

<sup>1</sup>*Key Laboratory for Microstructural Material Physics of Hebei Province,  
School of Science, Yanshan University, Qinhuangdao 066004, China*

<sup>2</sup>*School of Physics, Nanjing University, Nanjing 210093, China*

<sup>3</sup>*Beijing Computational Science Research Center, Beijing 100193, China*

<sup>4</sup>*School of Physics, Beihang University, Beijing 100191, China and*

<sup>5</sup>*Department of Physics, Beijing Normal University, Beijing 100875, China*

The renormalization of the electrons in cuprate superconductors is characterized by the kink in the quasiparticle dispersion. Here the bilayer coupling effect on the quasiparticle dispersion kink in the electron-doped bilayer cuprate superconductors is studied based on the kinetic-energy-driven superconductivity. It is shown that the kink in the quasiparticle dispersion is present all around the electron Fermi surface, as the quasiparticle dispersion kink in the single-layer case. However, in comparison with the corresponding single-layer case, the kink effect in the quasiparticle dispersion at around the antinodal region becomes the most pronounced, indicating that the kink effect in the quasiparticle dispersion at around the antinodal region is enhanced by the bilayer coupling.

PACS numbers: 74.25.Jb, 74.25.Dw, 74.20.Mn, 74.72.Ek

The parent compounds of cuprate superconductors are structurally characterized by the stacking  $\text{CuO}_2$  layers<sup>1,2</sup>, and then superconductivity emerges when charge carriers, holes or electrons, are doped into these  $\text{CuO}_2$  layers<sup>3-6</sup>. In both the electron- and hole-doped cuprate superconductors, the renormalization of the electrons to form the quasiparticles are due to the strong electron's coupling to various bosonic excitations<sup>7,8</sup>, and then the unconventional properties, including the exceptionally high superconducting (SC) transition temperature  $T_c$ , have often been attributed to particular characteristics of the quasiparticle excitations<sup>3-9</sup>.

The renormalization of the electrons is characterized by the kink in the quasiparticle dispersion<sup>3-6</sup>. In the hole-doped case, the kink in the quasiparticle dispersion was firstly observed in the angle-resolved photoemission spectroscopy (ARPES) measurements on the hole-doped bilayer cuprate superconductors<sup>10-14</sup>. Later, this quasiparticle dispersion kink is found to be present in all families of the hole-doped cuprate superconductors with one or more  $\text{CuO}_2$  layers per unit cell<sup>15-18</sup>. In particular, these experimental observations also show that the quasiparticle dispersion kink is particularly obvious in these hole-doped cuprate superconductors with two or more  $\text{CuO}_2$  layers per unit cell<sup>10-18</sup>, reflecting an experimental fact that the kink effect in the quasiparticle dispersion is enhanced by the strong coupling between the  $\text{CuO}_2$  layers in a unit cell. On the electron-doped side, both the doped electrons and the proper annealing process in a low-oxygen environment are required to induce the intrinsic aspects of the unconventional properties<sup>6,19,20</sup>. In this case, although the kink in the quasiparticle dispersion associated with the improper annealing condition has

been observed early<sup>21-24</sup>, the intrinsic kink effect associated with the proper annealing condition was observed recently<sup>25</sup>. Moreover, the evolution of the electronic structure with the electron doping in the electron-doped bilayer cuprate superconductors has been investigated very recently in terms of the ARPES measurements<sup>26</sup>, where the entire momentum-resolved energy spectrum in the lightly electron doped case has been directly visualized. This electron-doped bilayer cuprate superconductor is an ideal system to tackle the coupling effect between the  $\text{CuO}_2$  layers within a unit cell on the renormalization of the dispersion<sup>26</sup>, however, the experimental data of the quasiparticle dispersion kink in the electron-doped bilayer cuprate superconductors is still lacking to date. In other words, it is still unclear whether the kink effect in the quasiparticle dispersion of the electron-doped cuprate superconductors is enhanced by the coupling between the  $\text{CuO}_2$  layers within a unit cell or not?

In our recent work<sup>27</sup>, the quasiparticle dispersion kink in the electron-doped single-layer cuprate superconductors has been studied based on the kinetic-energy-driven superconductivity, where we have shown that although the optimized  $T_c$  in the electron-doped single-layer cuprate superconductors is much smaller than that in the hole-doped counterparts, the electron- and hole-doped single-layer cuprate superconductors rather resemble each other in the doping range of the SC dome, indicating an absence of the disparity between the phase diagrams of the electron- and hole-doped cuprate superconductors. Moreover, the quasiparticle dispersion is affected by the spin excitation, and then the kink in the quasiparticle dispersion is always accompanied by the corresponding inflection point in the total self-energy<sup>27</sup>. In this paper, we study the effect of the coupling between the  $\text{CuO}_2$  layers within a unit cell on the quasiparticle dispersion kink in the electron-doped bilayer superconductors along with this line, and show that the quasiparticle dispersion kink is present all around the elec-

\*E-mail: sntan@ysu.edu.cn

†E-mail: spfeng@bnu.edu.cn

tron Fermi surface (EFS), as the corresponding quasiparticle dispersion kink in the single-layer case<sup>27</sup>. However, in comparison with the corresponding single-layer case<sup>27</sup>, the kink effect in the quasiparticle dispersion at around the antinodal region becomes the most pronounced, which therefore indicates that the kink effect in the quasiparticle dispersion at around the antinodal region is enhanced by the bilayer coupling.

It is commonly accepted that the essential physics of the doped CuO<sub>2</sub> layer can be described by the  $t$ - $J$  model on a square lattice<sup>28</sup>. However, for the discussions of the bilayer coupling effect on the quasiparticle dispersion kink in the electron-doped bilayer cuprate superconductors, the single-layer  $t$ - $J$  model can be extended by the consideration of the bilayer coupling as<sup>29</sup>,

$$\begin{aligned}
H = & -t \sum_{l\hat{\eta}a\sigma} C_{la\sigma}^\dagger C_{l+\hat{\eta}a\sigma} + t' \sum_{l\hat{\tau}a\sigma} C_{la\sigma}^\dagger C_{l+\hat{\tau}a\sigma} \\
& - \sum_{la \neq b\sigma} t_\perp(l) C_{la\sigma}^\dagger C_{lb\sigma} + \mu \sum_{la\sigma} C_{la\sigma}^\dagger C_{la\sigma} \\
& + J \sum_{l\hat{\eta}a} \mathbf{S}_{la} \cdot \mathbf{S}_{l+\hat{\eta}a} + J_\perp \sum_{la \neq b} \mathbf{S}_{la} \cdot \mathbf{S}_{lb}, \quad (1)
\end{aligned}$$

where  $a(b) = 1, 2$ , is the CuO<sub>2</sub> layer index, the hopping integrals  $t < 0$  and  $t' < 0$  in the electron-doped side,  $\hat{\eta} = \pm\hat{x}, \pm\hat{y}$  represents the nearest-neighbor (NN) sites of the site  $l$ ,  $\hat{\tau} = \pm\hat{x} \pm \hat{y}$  represents the next NN sites of the site  $l$ ,  $C_{la\sigma}^\dagger$  ( $C_{la\sigma}$ ) is the electron creation (annihilation) operator,  $\mathbf{S}_l$  is the spin operator with its components  $S_l^x$ ,  $S_l^y$ , and  $S_l^z$ , and  $\mu$  is the chemical potential, while the momentum dependence of the bilayer hopping  $t_\perp(\mathbf{k})$  is given by<sup>30-34</sup>,

$$t_\perp(\mathbf{k}) = \frac{t_\perp}{4} (\cos k_x - \cos k_y)^2, \quad (2)$$

which therefore leads to that the bilayer magnetic exchange  $J_\perp = (t_\perp/t)^2 J$ .

This bilayer  $t$ - $J$  model (1) is supplemented by the local constraint  $\sum_\sigma C_{la\sigma}^\dagger C_{la\sigma} \geq 1$  to remove zero electron occupancy, which is different from the hole-doped case<sup>29</sup>, where the local constraint is subjected to remove double electron occupancy, and can be treated properly in terms of the charge-spin separation fermion-spin transformation<sup>35,36</sup>. However, for the application of this fermion-spin transformation to treat the local constraint in the electron-doped side, we can work in the hole representation via a particle-hole transformation  $C_{la\sigma} \rightarrow f_{la-\sigma}^\dagger$ . In this hole representation, the  $t$ - $J$  model (1) can be rewritten as<sup>27</sup>,

$$\begin{aligned}
H = & t \sum_{l\hat{\eta}a\sigma} f_{la\sigma}^\dagger f_{l+\hat{\eta}a\sigma} - t' \sum_{l\hat{\tau}a\sigma} f_{la\sigma}^\dagger f_{l+\hat{\tau}a\sigma} \\
& + \sum_{la \neq b\sigma} t_\perp(l) f_{la\sigma}^\dagger f_{lb\sigma} - \mu \sum_{la\sigma} f_{la\sigma}^\dagger f_{la\sigma} \\
& + J \sum_{l\hat{\eta}a} \mathbf{S}_{la} \cdot \mathbf{S}_{l+\hat{\eta}a} + J_\perp \sum_{la \neq b} \mathbf{S}_{la} \cdot \mathbf{S}_{lb}, \quad (3)
\end{aligned}$$

and then the local constraint of no zero electron occupancy in the electron representation  $\sum_\sigma C_{la\sigma}^\dagger C_{la\sigma} \geq 1$  is replaced by the local constraint of no double hole occupancy in the hole representation  $\sum_\sigma f_{la\sigma}^\dagger f_{la\sigma} \leq 1$ , where  $f_{la\sigma}^\dagger$  ( $f_{la\sigma}$ ) is the hole creation (annihilation) operator. According to the fermion-spin transformation<sup>35,36</sup>, the constrained hole operators  $f_{la\uparrow}$  and  $f_{la\downarrow}$  now can be decoupled as:  $f_{la\uparrow} = a_{la\uparrow}^\dagger S_{la}^-$  and  $f_{la\downarrow} = a_{la\downarrow}^\dagger S_{la}^+$ , where the spinful fermion operator  $a_{la\sigma} = e^{-i\Phi_{l\sigma}} a_{la}$  keeps track of the charge degree of freedom of the constrained hole together with some effects of spin configuration rearrangements due to the presence of the doped charge carrier itself, while the localized spin operator  $S_l$  keeps track of the spin degree of freedom of the constrained hole, and then the local constraint without double hole occupancy is satisfied in analytical calculations.

Within the bilayer  $t$ - $J$  model in the fermion-spin representation, the renormalization of the dispersion in the hole-doped bilayer cuprate superconductors<sup>29</sup> has been investigated based on the kinetic-energy-driven superconductivity<sup>36-39</sup>, where the kink effect in the quasiparticle dispersion is enhanced by the strong bilayer coupling. Following these previous discussions<sup>29</sup>, the hole normal and anomalous Green's functions of the bilayer  $t$ - $J$  model (3) in the bonding-antibonding representation can be obtained explicitly as,

$$G_\nu^{(f)}(\mathbf{k}, \omega) = \frac{1}{\omega - \varepsilon_{\nu\mathbf{k}}^{(f)} - \Sigma_{\nu\text{tot}}^{(f)}(\mathbf{k}, \omega)}, \quad (4a)$$

$$\Im_\nu^{(f)\dagger}(\mathbf{k}, \omega) = \frac{L_\nu^{(f)}(\mathbf{k}, \omega)}{\omega - \varepsilon_{\nu\mathbf{k}}^{(f)} - \Sigma_{\nu\text{tot}}^{(f)}(\mathbf{k}, \omega)}, \quad (4b)$$

where  $\nu = 1, 2$  with  $\nu = 1$  ( $\nu = 2$ ) that represents the corresponding bonding (antibonding) component, the bare hole dispersion  $\varepsilon_{\nu\mathbf{k}}^{(f)} = \varepsilon_{\mathbf{k}}^{(f)} + (-1)^\nu t_\perp(\mathbf{k})$ , with  $\varepsilon_{\mathbf{k}}^{(f)} = -4t\gamma_{\mathbf{k}} + 4t'\gamma'_{\mathbf{k}} + \mu$ ,  $\gamma_{\mathbf{k}} = (\cos k_x + \cos k_y)/2$ , and  $\gamma'_{\mathbf{k}} = \cos k_x \cos k_y$ , while the hole total self-energy  $\Sigma_{\nu\text{tot}}^{(f)}(\mathbf{k}, \omega)$  is a specific combination of the hole normal self-energy  $\Sigma_{\nu\text{ph}}^{(f)}(\mathbf{k}, \omega)$  in the particle-hole channel and the hole anomalous self-energy  $\Sigma_{\nu\text{pp}}^{(f)}(\mathbf{k}, \omega)$  in the particle-particle channel as,

$$\Sigma_{\nu\text{tot}}^{(f)}(\mathbf{k}, \omega) = \Sigma_{\nu\text{ph}}^{(f)}(\mathbf{k}, \omega) + \frac{|\Sigma_{\nu\text{pp}}^{(f)}(\mathbf{k}, \omega)|^2}{\omega + \varepsilon_{\nu\mathbf{k}}^{(f)} + \Sigma_{\nu\text{ph}}^{(f)}(\mathbf{k}, -\omega)}, \quad (5)$$

and the function  $L_\nu^{(f)}(\mathbf{k}, \omega)$  is given by,

$$L_\nu^{(f)}(\mathbf{k}, \omega) = -\frac{\Sigma_{\nu\text{pp}}^{(f)}(\mathbf{k}, \omega)}{\omega + \varepsilon_{\nu\mathbf{k}}^{(f)} + \Sigma_{\nu\text{ph}}^{(f)}(\mathbf{k}, -\omega)}, \quad (6)$$

where hole normal self-energy  $\Sigma_{\nu\text{ph}}^{(f)}(\mathbf{k}, \omega)$  and hole anomalous self-energy  $\Sigma_{\nu\text{pp}}^{(f)}(\mathbf{k}, \omega)$  have been given explicitly in Ref. 29 except for  $t < 0$  and  $t' < 0$  in the electron-doped side.

Our main goal is to derive explicitly the electron normal and anomalous Green's functions  $G_\nu(\mathbf{k}, \omega)$  and  $\Im_\nu^\dagger(\mathbf{k}, \omega)$  of the  $t$ - $J$  model (1), which are directly associated with the hole normal and anomalous Green's functions  $G_\nu^{(f)}(\mathbf{k}, \omega)$  and  $\Im_\nu^{(f)\dagger}(\mathbf{k}, \omega)$  in Eq. (4) via the particle-hole transformation  $C_{la\sigma} \rightarrow f_{la-\sigma}^\dagger$  as  $G(l-l', t-t') = \langle\langle C_{l\sigma}(t); C_{l'\sigma}^\dagger(t') \rangle\rangle = \langle\langle f_{l\sigma}^\dagger(t); f_{l'\sigma}(t') \rangle\rangle = -G^{(f)}(l'-l, t'-t)$  and  $\Im(l-l', t-t') = \langle\langle C_{l\downarrow}(t); C_{l'\uparrow}^\dagger(t') \rangle\rangle = \langle\langle f_{l\uparrow}^\dagger(t); f_{l'\downarrow}^\dagger(t') \rangle\rangle = \Im^{(f)\dagger}(l-l', t-t')$ . With the helps of the above hole normal and anomalous Green's functions (4), the electron normal and anomalous Green's functions in the bonding-antibonding representation can be derived as<sup>27</sup>  $G_\nu(\mathbf{k}, \omega) = -G_\nu^{(f)}(\mathbf{k}, -\omega)$  and  $\Im_\nu(\mathbf{k}, \omega) = \Im_\nu^{(f)\dagger}(\mathbf{k}, \omega)$ , respectively, with the bare electron dispersion  $\varepsilon_{\mathbf{k}}^{(\nu)}$ , the electron normal self-energy  $\Sigma_{\text{ph}}^{(\nu)}(\mathbf{k}, \omega)$ , and the electron anomalous self-energy  $\Sigma_{\text{pp}}^{(\nu)}(\mathbf{k}, \omega)$  that can be obtained as  $\varepsilon_{\mathbf{k}}^{(\nu)} = -\varepsilon_{\nu\mathbf{k}}^{(f)}$ ,  $\Sigma_{\text{ph}}^{(\nu)}(\mathbf{k}, \omega) = -\Sigma_{\nu\text{ph}}^{(f)}(\mathbf{k}, -\omega)$ , and  $\Sigma_{\text{pp}}^{(\nu)}(\mathbf{k}, \omega) = \Sigma_{\nu\text{pp}}^{(f)}(\mathbf{k}, \omega)$ , respectively. In this case, the electron spectral function  $A_\nu(\mathbf{k}, \omega) = -2\text{Im}G_\nu(\mathbf{k}, \omega)$  in the bonding-antibonding representation now can be obtained explicitly as,

$$A_\nu(\mathbf{k}, \omega) = \frac{-2\text{Im}\Sigma_{\text{tot}}^{(\nu)}(\mathbf{k}, \omega)}{[\omega - \varepsilon_{\mathbf{k}}^{(\nu)} - \text{Re}\Sigma_{\text{tot}}^{(\nu)}(\mathbf{k}, \omega)]^2 + [\text{Im}\Sigma_{\text{tot}}^{(\nu)}(\mathbf{k}, \omega)]^2}, \quad (7)$$

with the electron total self-energy  $\Sigma_{\text{tot}}^{(\nu)}(\mathbf{k}, \omega)$ ,

$$\Sigma_{\text{tot}}^{(\nu)}(\mathbf{k}, \omega) = \Sigma_{\text{ph}}^{(\nu)}(\mathbf{k}, \omega) + \frac{|\Sigma_{\text{pp}}^{(\nu)}(\mathbf{k}, \omega)|^2}{\omega + \varepsilon_{\mathbf{k}}^{(\nu)} + \Sigma_{\text{ph}}^{(\nu)}(\mathbf{k}, -\omega)}, \quad (8)$$

where  $\text{Re}\Sigma_{\text{tot}}^{(\nu)}(\mathbf{k}, \omega)$  and  $\text{Im}\Sigma_{\text{tot}}^{(\nu)}(\mathbf{k}, \omega)$  are the real and imaginary parts of the electron total self-energy, respectively. As we have shown in the previous studies<sup>27</sup> that in the numerical calculation at a finite lattice, the sharp peak visible for temperature  $T \rightarrow 0$  in the electron normal (anomalous) self-energy is actually a  $\delta$ -functions, broadened by a small damping. The calculation in this paper for the electron normal (anomalous) self-energy is performed numerically on a  $120 \times 120$  lattice in momentum space, with the infinitesimal  $i0_+ \rightarrow i\Gamma$  replaced by a small damping  $\Gamma = 0.05J$ . In the following discussions, we fix the parameters  $t/J = -2.5$ ,  $t'/t = 0.22$ , and  $t_\perp/t = 0.1$  in the bilayer  $t$ - $J$  model (1), and then all the energy scales are in the units of  $J = 1$ . However, to compare with the single-layer case, we use  $J = 100$  meV. All these values of the parameters are the typical values of the electron-doped cuprate superconductors<sup>6,26</sup>.

In cuprate superconductors, the topology of EFS plays an essential role in the understanding of the unconventional properties, since everything happens at around EFS. In particular, the strong coupling between the electrons and a strongly dispersive spin excitation in cuprate superconductors leads to a strong redistribution of the spectral weights on EFS<sup>27,29</sup>, and then a bewildering variety of electronically ordered states is driven by this

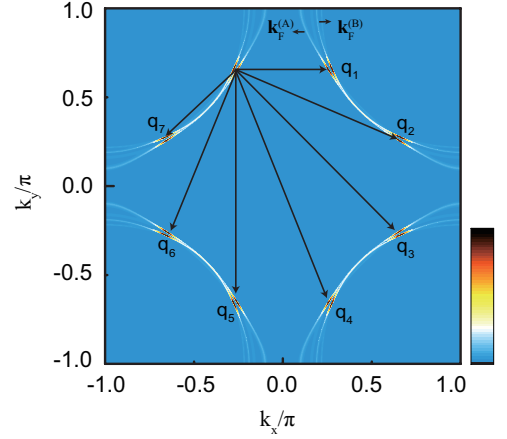


FIG. 1: (Color online) The intensity map of the bonding and antibonding components of the electron spectral function  $A_1(\mathbf{k}, 0)$  and  $A_2(\mathbf{k}, 0)$  at zero binding-energy in  $\delta = 0.15$  with  $T = 0.002J$  for  $t/J = -2.5$ ,  $t'/t = 0.22$ , and  $t_\perp/t = 0.1$ .

EFS instability<sup>40–43</sup>. However, as shown in Eq. (7), the electron spectral function in the electron-doped bilayer cuprate superconductors has been separated into its bonding and antibonding components due to the presence of the bilayer coupling, which leads to two EFS contours  $\mathbf{k}_F^{(B)}$  and  $\mathbf{k}_F^{(A)}$  deriving directly from the bonding and antibonding layers. For a convenience in the following discussions of the bilayer coupling effect on the quasiparticle dispersion kink, we firstly plot the EFS map from both the bonding component  $A_1(\mathbf{k}, 0)$  and the antibonding component  $A_2(\mathbf{k}, 0)$  of the electron spectral function (7) at zero binding-energy for  $\delta = 0.15$  with  $T = 0.002J$  in Fig. 1, where in corresponding to the momentum dependence of the interlayer hopping in Eq. (2), the maximal distance between the bonding and antibonding EFS contours  $\mathbf{k}_F^{(B)}$  and  $\mathbf{k}_F^{(A)}$  appears at around the antinodal region, then it gradually reduces when the momentum moves away from the antinodal region, and it eventually disappears at around the nodal region, indicating that the bilayer coupling with the high impacts on the electronic structure mainly occurs at around antinodal region. Apart from this intrinsic feature, another intrinsic feature is the redistribution of the spectral weights in the bonding and antibonding EFS contours, where the spectral weight on  $\mathbf{k}_F^{(B)}$  ( $\mathbf{k}_F^{(A)}$ ) at around the bonding (antibonding) antinodal region is reduced greatly. As a natural consequence, the bonding (antibonding) EFS contour is broken up into the disconnected bonding (antibonding) Fermi arcs located at around the bonding (antibonding) nodal region. However, the renormalization from the quasiparticle scattering further reduces the most part of the spectral weight on the bonding (antibonding) Fermi arcs to the tips of the bonding (antibonding) Fermi arcs<sup>42,43</sup>, and then these tips of the Fermi arcs connected by the scattering wave vectors  $\mathbf{q}_i$  shown in Fig. 1 construct an octet scattering model. In this

case, a bewildering variety of electronic orders described by the quasiparticle scattering processes with the scattering wave vectors  $\mathbf{q}_i$  therefore is driven by this EFS instability<sup>40–43</sup>. These intrinsic features of the EFS reconstruction resemble these obtained for the corresponding hole-doped case<sup>29</sup>.

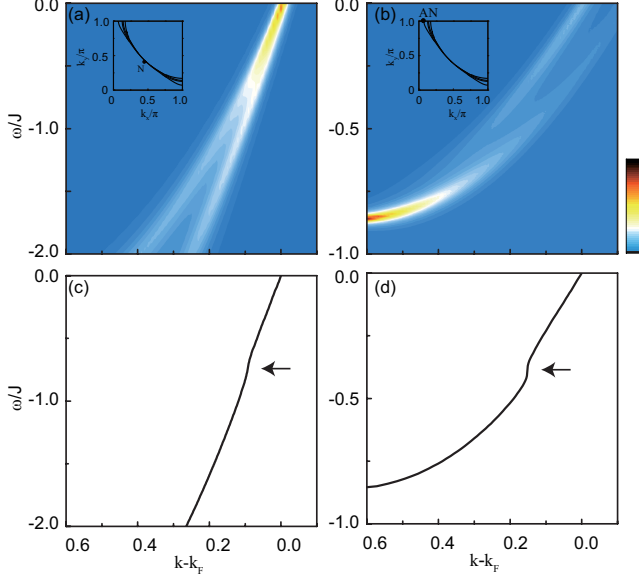


FIG. 2: (Color online) Upper panel: the intensity maps of the antibonding component of the electron spectral function as a function of binding-energy along (a) the nodal cut and (b) the antinodal cut at  $\delta = 0.15$  with  $T = 0.002J$  for  $t/J = -2.5$ ,  $t'/t = 0.22$ , and  $t_{\perp}/t = 0.1$ . Lower panel: the antibonding quasiparticle dispersions along (c) the nodal cut and (d) the antinodal cut extracted from the positions of the lowest-energy quasiparticle excitation peaks in (a) and (b), respectively. The arrow indicates the kink position.

We are now ready to discuss the bilayer coupling effect on the quasiparticle dispersion kink in the electron-doped bilayer cuprate superconductors. In the upper panel of Fig. 2, we plot the intensity map of the antibonding component  $A_2(\mathbf{k}, \omega)$  of the electron spectral function as a function of binding-energy along (a) the nodal cut and (b) the antinodal cut at  $\delta = 0.15$  with  $T = 0.002J$ , while the corresponding antibonding quasiparticle dispersions along (c) the nodal cut and (d) the antinodal cut extracted from the positions of the lowest-energy quasiparticle excitation peaks in (a) and (b), respectively, are shown in the lower panel. It is shown clearly that although the kink in the quasiparticle dispersion is present all around the antibonding EFS, the quasiparticle dispersive behavior at around the nodal region is much different from that at around the antinodal region. The results in Fig. 2a and Fig. 2c show that the quasiparticle dispersion along the nodal cut at both the low binding-energy and high binding-energy ranges exhibits a linear behavior, but with different slopes, and then these two ranges with different slopes are separated by a weak kink. In particular, for the low binding-energy less

than the kink energy, the spectrum exhibits sharp peaks with a weak dispersion, while for the high binding-energy greater than the kink energy, the spectrum exhibits broad peaks with a stronger dispersion, as the renormalization of the dispersion in the single-layer case<sup>27</sup>. However, the kink effect in the quasiparticle dispersion of the electron-doped bilayer cuprate superconductors at around the antinodal region is more stronger than that in the single-layer case. This follows a basic fact that at the kink energy, although the quasiparticle dispersion of the electron-doped single-layer cuprate superconductors at around the antinodal region is broken up into a fast dispersive high binding-energy part and a slow dispersive low binding-energy part<sup>27</sup>, this breaking effect becomes the most pronounced in the electron-doped bilayer cuprate superconductors as shown in Fig. 2b and Fig. 2d, which shows that the kink effect in the quasiparticle dispersion of the electron-doped bilayer cuprate superconductors at around the antinodal region is enhanced. Concomitantly, the quasiparticle dispersion kink emerges in the energy  $\omega_{\text{kink}} \sim 0.72J = 72$  meV at around the nodal region, while the quasiparticle dispersion kink occurs in the energy  $\omega_{\text{kink}} \sim 0.39J = 39$  meV at around the antinodal region, which therefore indicates that the characteristic kink energy decreases gradually when the momentum moves from the nodal region to the antinodal region, in qualitative agreement with these in the single-layer case<sup>27</sup>. Our present result of the enhancement of the kink effect in the quasiparticle dispersion of the electron-doped bilayer cuprate superconductors is also qualitatively consistent with that in the hole-doped bilayer cuprate superconductors<sup>29</sup>, suggesting a common quasiparticle dispersion kink mechanism for both the electron- and hole-doped cuprate superconductors.

The essential physics of the kink effect in the quasiparticle dispersion of the electron-doped bilayer cuprate superconductors and of its enhancement at around the antinodal region is the same as that in the corresponding hole-doped case<sup>29</sup>. On the one hand, the emergence of the quasiparticle dispersion kink in the electron-doped bilayer cuprate superconductors can be also attributed to the electron self-energy effects arising from the strong electron's coupling to a strongly dispersive spin excitation, as the emergence of the quasiparticle dispersion kink in the single-layer case<sup>27</sup>. To see this point more clearly, we plot the real part of the antibonding total self-energy  $\text{Re}\Sigma_{\text{tot}}^{(2)}(\mathbf{k}, \omega)$  as a function of binding-energy along (a) the nodal dispersion and (b) the antinodal dispersion as shown in Fig. 2c and Fig. 2d, respectively, at  $\delta = 0.15$  with  $T = 0.002J$  in the upper panel of Fig. 3, where the red arrow indicates the inflection point (then the point of the slope change). In the lower panel, we plot the corresponding imaginary part of the antibonding total self-energy  $\text{Im}\Sigma_{\text{tot}}^{(2)}(\mathbf{k}, \omega)$  (then the antibonding quasiparticle scattering rate) as a function of binding-energy along (c) the nodal dispersion and (d) the antinodal dispersion, where the blue arrow denotes the peak position (then the point of the drop in the spectral weight at around

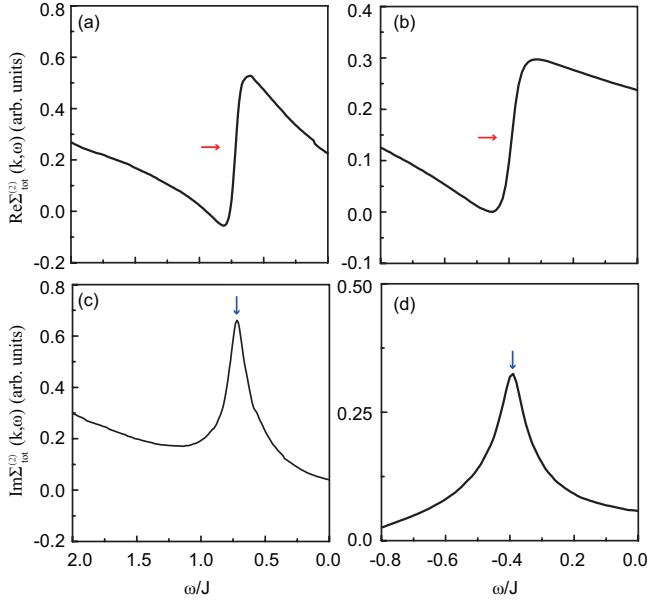


FIG. 3: (Color online) Upper panel: the real part of the antibonding total self-energy as a function of binding-energy along (a) the nodal dispersion and (b) the antinodal dispersion at  $\delta = 0.15$  with  $T = 0.002J$  for  $t/J = -2.5$ ,  $t'/t = 0.22$ , and  $t_{\perp}/t = 0.1$ . Lower panel: the corresponding imaginary part of the antibonding total self-energy as a function of binding-energy along (c) the nodal dispersion and (d) the antinodal dispersion. The red arrow indicates inflection point, while the blue arrow denotes the peak position.

the quasiparticle dispersion kink). Obviously, there is a slope change in the real part of the antibonding total self-energy  $\text{Re}\Sigma_{\text{tot}}^{(2)}(\mathbf{k}, \omega)$ . However, in the corresponding to this slope change, a peak structure appears simultaneously in the imaginary part of the antibonding total self-energy  $\text{Im}\Sigma_{\text{tot}}^{(2)}(\mathbf{k}, \omega)$ . These results thus show that the quasiparticle dispersion kink is induced by the slope change in  $\text{Re}\Sigma_{\text{tot}}^{(2)}(\mathbf{k}, \omega)$ , i.e., the position of the quasiparticle dispersion kink shown in Fig. 2 is exactly the same as that for the corresponding inflection point in  $\text{Re}\Sigma_{\text{tot}}^{(2)}(\mathbf{k}, \omega)$  shown in Fig. 3. This is why the kink in the quasiparticle dispersion marks the crossover between two different slopes. Moreover, the position of the quasiparticle dispersion kink shown in Fig. 2 is also the exactly same as that for the corresponding peak in the imaginary part of the antibonding total self-energy  $\text{Im}\Sigma_{\text{tot}}^{(2)}(\mathbf{k}, \omega)$  shown in Fig. 3, i.e., there is an exact one to one correspondence between the kink position shown in Fig. 2 and the peak position in  $\text{Im}\Sigma_{\text{tot}}^{(2)}(\mathbf{k}, \omega)$  shown in Fig. 3, which therefore shows that the spectral weight at around the

quasiparticle dispersion kink is reduced strongly by the corresponding peak in  $\text{Im}\Sigma_{\text{tot}}^{(2)}(\mathbf{k}, \omega)$ , and then the weak spectral intensity appears always at around the quasiparticle dispersion kink. On the other hand, the bilayer coupling in Eq. (2) is absent at around the nodal region, and then the less visible kink in the antibonding quasiparticle dispersion is caused mainly by the renormalization of the electrons within a  $\text{CuO}_2$  layer. However, at around the antinodal region, the bilayer coupling exhibits its largest value, this large band splitting lead to that the break separating of the fast dispersive high-energy part from the slow dispersive low-energy part more stronger. This strong separation of the quasiparticle dispersion at the kink energy results in the enhancement of the kink effect in the quasiparticle dispersion of the electron-doped bilayer cuprate superconductors at around the antinodal region. In other words, the kink effect in the quasiparticle dispersion of the electron-doped bilayer cuprate superconductors at around the antinodal region becomes the most pronounced due to the presence of the bilayer coupling.

In conclusion, within the framework of the kinetic-energy driven superconductivity, we have studied the bilayer coupling effect on the quasiparticle dispersion kink in the electron-doped bilayer cuprate superconductors. Our results show that the kink in the quasiparticle dispersion is present all around the antibonding EFS, as the corresponding quasiparticle dispersion kink in the electron-doped single-layer cuprate superconductors. However, in comparison with the corresponding case in the electron-doped single-layer cuprate superconductors, the kink effect in the quasiparticle dispersion of the electron-doped bilayer cuprate superconductors at around the antinodal region becomes the most pronounced, which therefore indicates that the kink effect in the quasiparticle dispersion of the electron-doped bilayer cuprate superconductors at around the antinodal region is enhanced by the bilayer coupling.

### Acknowledgements

ST is supported by Research Foundation of Yanshan University under Grant No. 8190448. HG is supported by NSFC under Grant Nos. 11774019 and 12074022, and the Fundamental Research Funds for the Central Universities and HPC resources at Beihang University. SF are supported by the National Key Research and Development Program of China, and the National Natural Science Foundation of China (NSFC) under Grant Nos. 11974051 and 11734002.

<sup>1</sup> J. G. Bednorz and K. A. Müller, Z. Phys. B **64**, 189 (1986).

<sup>2</sup> Y. Tokura, H. Takagi, and S. Uchida, Nature **337**, 345 (1989).

<sup>3</sup> See, e.g., the review, A. Damascelli, Z. Hussain, and Z.-X. Shen, Rev. Mod. Phys. **75**, 473 (2003).

<sup>4</sup> See, e.g., the review, J. C. Campuzano, M. R. Norman, M.

- Randeira, in *Physics of Superconductors*, vol. II, edited by K. H. Bennemann and J. B. Ketterson (Springer, Berlin Heidelberg New York, 2004), p. 167.
- <sup>5</sup> See, e.g., the review, J. Fink, S. Borisenko, A. Kordyuk, A. Koitzsch, J. Geck, V. Zabolotnyy, M. Knupfer, B. Buechner, and H. Berger, in *Lecture Notes in Physics*, vol. 715, edited by S. Hüfner (Springer-Verlag Berlin Heidelberg, 2007), p. 295.
  - <sup>6</sup> See, e.g., the review, N. P. Armitage, P. Fournier, and R. L. Greene, *Rev. Mod. Phys.* **82**, 2421 (2010).
  - <sup>7</sup> See, e.g., the review, J. P. Carbotte, T. Timusk, and J. Hwang, *Rep. Prog. Phys.* **74**, 066501 (2011).
  - <sup>8</sup> J. M. Bok, J. J. Bae, H. Y. Choi, C. M. Varma, W. Zhang, J. He, Y. Zhang, L. Yu, and X. J. Zhou, *Sci. Adv.* **2**, e1501329 (2016).
  - <sup>9</sup> See, e.g., the review, J.-X. Yin, S. H. Pan, M. Z. Hasan, *Nat. Rev. Phys.* **3**, 249 (2021).
  - <sup>10</sup> P. V. Bogdanov, A. Lanzara, S. A. Kellar, X. J. Zhou, E. D. Lu, W. J. Zheng, G. Gu, J.-I. Shimoyama, K. Kishio, H. Ikeda, R. Yoshizaki, Z. Hussain, and Z. X. Shen, *Phys. Rev. Lett.* **85**, 2581 (2000).
  - <sup>11</sup> A. Kaminski, M. Randeria, J. C. Campuzano, M. R. Norman, H. Fretwell, J. Mesot, T. Sato, T. Takahashi, and K. Kadowaki, *Phys. Rev. Lett.* **86**, 1070 (2001).
  - <sup>12</sup> P. D. Johnson, T. Valla, A. V. Fedorov, Z. Yusof, B. O. Wells, Q. Li, A. R. Moodenbaugh, G. D. Gu, N. Koshizuka, C. Kendziora, Sha Jian, and D. G. Hinks, *Phys. Rev. Lett.* **87**, 177007 (2001).
  - <sup>13</sup> T. Sato, H. Matsui, T. Takahashi, H. Ding, H.-B. Yang, S.-C. Wang, T. Fujii, T. Watanabe, A. Matsuda, T. Terashima, and K. Kadowaki, *Phys. Rev. Lett.* **91**, 157003 (2003).
  - <sup>14</sup> A. A. Kordyuk, S. V. Borisenko, V. B. Zabolotnyy, J. Geck, M. Knupfer, J. Fink, B. Büchner, C. T. Lin, B. Keimer, H. Berger, A. V. Pan, Seiki Komiya, and Yoichi Ando, *Phys. Rev. Lett.* **97**, 017002 (2006).
  - <sup>15</sup> X. J. Zhou, T. Yoshida, A. Lanzara, P. V. Bogdanov, S. A. Kellar, K. M. Shen, W. L. Yang, F. Ronning, T. Sasagawa, T. Kakeshita, T. Noda, H. Eisaki, S. Uchida, C. T. Lin, F. Zhou, J. W. Xiong, W. X. Ti, Z. X. Zhao, A. Fujimori, Z. Hussain, and Z.-X. Shen, *Nature* **423**, 398 (2003).
  - <sup>16</sup> T. Yoshida, X. J. Zhou, D. H. Lu, Seiki Komiya, Yoichi Ando, H. Eisaki, T. Kakeshita, S. Uchida, Z. Hussain, Z.-X. Shen and A. Fujimori, *J. Phys.: Condens. Matter* **19**, 125209 (2007).
  - <sup>17</sup> W. S. Lee, K. Tanaka, I. M. Vishik, D. H. Lu, R. G. Moore, H. Eisaki, A. Iyo, T. P. Devereaux, and Z. X. Shen, *Phys. Rev. Lett.* **103**, 067003 (2009).
  - <sup>18</sup> Y. Chen, A. Iyo, W. Yang, A. Ino, M. Arita, S. Johnston, H. Eisaki, H. Namatame, M. Taniguchi, T. P. Devereaux, Z. Hussain, and Z.-X. Shen, *Phys. Rev. Lett.* **103**, 036403 (2009).
  - <sup>19</sup> T. Adachi, Y. Mori, A. Takahashi, M. Kato, T. Nishizaki, T. Sasaki, N. Kobayashi, and Y. Koike, *J. Phys. Soc. Jpn.* **82**, 063713 (2013).
  - <sup>20</sup> See, e.g., the review, T. Adachi, T. Kawamata, Y. Koike, *Condensed Matter* **2**, 23 (2017).
  - <sup>21</sup> A. F. Santander-Syro, T. Kondo, J. Chang, A. Kaminski, S. Pailhes, M. Shi, L. Patthey, A. Zimmers, B. Liang, P. Li, R. L. Greene, arXiv:0903.3413.
  - <sup>22</sup> F. Schmitt, W. S. Lee, D.-H. Lu, W. Meevasana, E. Motoyama, M. Greven, and Z.-X. Shen, *Phys. Rev. B* **78**, 100505(R) (2008).
  - <sup>23</sup> S. R. Park, D. J. Song, C. S. Leem, C. Kim, C. Kim, B. J. Kim, and H. Eisaki, *Phys. Rev. Lett.* **101**, 117006 (2008).
  - <sup>24</sup> N. P. Armitage, D. H. Lu, C. Kim, A. Damascelli, K. M. Shen, F. Ronning, D. L. Feng, P. Bogdanov, X. J. Zhou, W. L. Yang, Z. Hussain, P. K. Mang, N. Kaneko, M. Greven, Y. Onose, Y. Taguchi, Y. Tokura, and Z.-X. Shen, *Phys. Rev. B* **68**, 064517 (2003).
  - <sup>25</sup> M. Horio, K. P. Kramer, Q. Wang, A. Zaidan, K. von Arx, D. Sutter, C. E. Matt, Y. Sassa, N. C. Plumb, M. Shi, A. Hanff, S. K. Mahatha, H. Bentmann, F. Reinert, S. Rohlf, F. K. Diekmann, J. Buck, M. Kalläne, K. Rossnagel, E. Rienks, V. Granata, R. Fittipaldi, A. Vecchione, T. Ohgi, T. Kawamata, T. Adachi, Y. Koike, A. Fujimori, M. Hoesch, J. Chang, arXiv:2006.13119.
  - <sup>26</sup> C. Hu, J. Zhao, Q. Gao, H. Yan, H. Rong, J. Huang, J. Liu, Y. Cai, C. Li, H. Chen, L. Zhao, G. Liu, C. Jin, Z. Xu, T. Xiang, and X. J. Zhou, *Nat. Commun.* **12**, 1356 (2021).
  - <sup>27</sup> S. Tan, Y. Liu, Y. Mou, and S. Feng, *Phys. Rev. B* **103**, 014503 (2021).
  - <sup>28</sup> P. W. Anderson, *Science* **235**, 1196 (1987).
  - <sup>29</sup> Y. Liu, Y. Lan, Y. Mou, and S. Feng, *Physica C* **576**, 1353661 (2020).
  - <sup>30</sup> S. Massida, J. Yu, and A. J. Freeman, *Physica C* **152**, 251 (1988).
  - <sup>31</sup> S. Chakravarty, A. Sudbø, P. W. Anderson, and S. Strong, *Science* **261**, 337 (1993).
  - <sup>32</sup> O. K. Andersen, O. Jepsen, A. I. Liechtenstein, and I. I. Mazin, *Phys. Rev. B* **49**, 4145 (1994).
  - <sup>33</sup> O. K. Andersen, A. I. Liechtenstein, O. Jepsen, and F. Paulsen, *J. Phys. Chem. Solids* **56**, 1573 (1995).
  - <sup>34</sup> A. I. Liechtenstein, O. Gunnarsson, O. K. Andersen, and R. M. Martin, *Phys. Rev. B* **54**, 12505 (1996).
  - <sup>35</sup> S. Feng, J. Qin, and T. Ma, *J. Phys.: Condens. Matter* **16**, 343 (2004); S. Feng, Z. B. Su, and L. Yu, *Phys. Rev. B* **49**, 2368 (1994).
  - <sup>36</sup> See, e.g., the review, S. Feng, Y. Lan, H. Zhao, L. Kuang, L. Qin, and X. Ma, *Int. J. Mod. Phys. B* **29**, 1530009 (2015).
  - <sup>37</sup> S. Feng, *Phys. Rev. B* **68**, 184501 (2003); S. Feng, T. Ma, and H. Guo, *Physica C* **436**, 14 (2006).
  - <sup>38</sup> S. Feng, H. Zhao, and Z. Huang, *Phys. Rev. B* **85**, 054509 (2012); *Phys. Rev. B* **85**, 099902(E) (2012).
  - <sup>39</sup> S. Feng, L. Kuang, and H. Zhao, *Physica C* **517**, 5 (2015).
  - <sup>40</sup> E. H. da Silva Neto, R. Comin, F. He, R. Sutarto, Y. Jiang, R. L. Greene, G. A. Sawatzky, and A. Damascelli, *Science* **347**, 282 (2015).
  - <sup>41</sup> E. H. da Silva Neto, B. Yu, M. Minola, R. Sutarto, E. Schierle, F. Boschini, M. Zonno, M. Bluschke, J. Higgins, Y. Li, G. Yu, E. Weschke, F. He, M. L. Tacon, R. L. Greene, M. Greven, G. A. Sawatzky, B. Keimer, and A. Damascelli, *Sci. Adv.* **2**, e1600782 (2016).
  - <sup>42</sup> M. Horio, T. Adachi, Y. Mori, A. Takahashi, T. Yoshida, H. Suzuki, L. C. C. Ambolode II, K. Okazaki, K. Ono, H. Kumigashira, H. Anzai, M. Arita, H. Namatame, M. Taniguchi, D. Ootsuki, K. Sawada, M. Takahashi, T. Mizokawa, Y. Koike and A. Fujimori, *Nat. Commun.* **7**, 10567 (2016).
  - <sup>43</sup> Y. Mou and S. Feng, *Phil. Mag.* **97**, 3361 (2017); S. Tan, Y. Mou, Y. Liu, and S. Feng, *J. Supercond. Nov. Magn.* **33**, 2305 (2020).